Bandwidth-limited control of orbital and magnetic orders in half-doped manganites by epitaxial strain

D. Gutiérrez,[1] G. Radaelli,[1,2,*] F. Sánchez,[1] R. Bertacco,[2] and J. Fontcuberta[1,†]

[1]*Institut de Ciència de Materials de Barcelona (ICMAB-CSIC), Campus UAB, 08193 Bellaterra, Catalonia, Spain*

[2]*LNESS, Dipartimento di Fisica, Politecnico di Milano, 22100 Como, Italy*

(Received 24 October 2013; published 6 February 2014)

The magnetotransport phase diagram of half-doped manganites $Ln_{0.5}A_{0.5}MnO_3$ (Ln = La^{3+}, Nd^{3+}, etc., and A = Sr^{2+}, Ca^{2+}, etc.) is primarily dictated by the bare conduction bandwith (W_0), which itself is controlled by the Mn-O-Mn bond angle, and the carrier concentration. In thin films, epitaxial strain (ε) provides an additional tool to tune W_0 by selecting orbital ordering at fixed carrier concentration. Here, we will show that compressive or tensile epitaxial strain on half-doped manganites can have a tremendous and distinct effect on $La_{0.5}Sr_{0.5}MnO_3$ (LSMO5) and $La_{0.5}Ca_{0.5}MnO_3$ (LCMO5), having broad or narrow W_0, respectively. It is found that in LSMO5, large compressive strain triggers a change from a ferromagnetic and metallic ground state to an insulating and antiferromagnetic state whereas a tensile strain produces an antiferromagnetic but metallic state. In contrast, under strain, LCMO5 remains an antiferromagnetic insulator irrespectively of the strain state. These results illustrate that orbital ordering largely depends on the interplay between W_0 and ε and provide a guideline towards responsive manganite layers.

DOI: 10.1103/PhysRevB.89.075107 PACS number(s): 75.47.Lx, 75.47.Gk, 75.70.Ak

I. INTRODUCTION

Half-doped manganites $La_{0.5}A_{0.5}MnO_3$ (A is a divalent ion) have recently attracted renewed attention because their ground state [ferromagnetic (FM) or antiferromagnetic (AF), metallic (M) or insulator (I)] can be easily modified by engineering the bandwidth (W_0) or modifying the carrier density. This property makes half-doped manganites ideal materials to be integrated in reconfigurable tunnel junctions with potentially large electroresistance [1]. Indeed, recent reports showed record tunnel electroresistance (TER) values where half-doped manganites are combined with ferroelectric tunneling [2]. In these heterostructures, the piezoresponse and polarization surface charges of the ferroelectric layer both can contribute to modify the properties of the adjacent manganite layer and thus those of the tunnel barrier. Progress in this direction and discrimination between strain and field effects in ferroelectric/half-doped heterostructures require detailed understanding of the epitaxial strain effects on the properties of half-doped manganite ultrathin films.

It is established that in manganites, the magnetic and the orbital degrees of freedom are strongly coupled. This coupling allows the control of the orbital order by applying a magnetic field, but the reverse process is also possible: magnetic order can be indirectly controlled, via orbital order, by the lattice distortion. One noticeable example is the drastic modification of the ground state of the large W_0 $La_{0.5}Sr_{0.5}MnO_3$ (LSMO5) obtained by Konishi *et al.* [3] by growing thin films on different substrates and so controlling the tetragonality [c/a, where (a, c) are the in-plane and out-of-plane unit cell parameters, respectively]. By changing c/a only from 1.04 (in-plane compressive strain, $\varepsilon < 0$) to 0.98 (in-plane tensile strain, $\varepsilon > 0$), the LSMO5 follows a sequence of different ground states: from the insulating and antiferromagnetic C-type AF, to the metallic and ferromagnetic F-FM, and finally to an in-plane conducting and antiferromagnetic A-type AF phase, in good agreement with the phase diagram obtained by first-principles band-structure calculations [4,5]. Still, the question of whether the A-AF phase remains stable and metallic under larger tensile strain ($c/a < 0.98$)—which is expected to promote the narrowing of the quasi-two-dimensional conduction band—remains open.

In contrast to LSMO5, calculations of the effect of tetragonal distortion c/a on the phase diagram of narrower W_0 oxides, such as $La_{0.5}Ca_{0.5}MnO_3$ (LCMO5), are not yet available, most likely due to the existence of complex charge ordering (CO) and electronic phase separation (PS) phenomena, discussed at length in the literature [5–7], here favored by the bandwidth narrowing induced by the smaller Ca^{2+} ions at A sites in the $La_{0.5}A_{0.5}MnO_3$ perovskite. In brief, upon cooling, bulk LCMO5 undergoes first a paramagnetic to FM transition and, at lower temperature, a simultaneous AF and CO transition. Experimentally, strain effects on LCMO5 thin films are much less known. LCMO5 films on different substrates have been reported [8–10] and there is consensus that PS occurs and, maybe not so surprisingly, properties of films are found to strongly vary depending on growth conditions and thickness. However, more work needs to be done on strain effects on magnetic and transport properties on LCMO5 films.

Here, we report on systematic investigation of the magnetic and transport properties of LSMO5 and LCMO5 thin films of different thicknesses and grown on different substrates ($DyScO_3$, $SrTiO_3$, (La,Sr)(Al,Ta)O_3, $LaAlO_3$, and $YAlO_3$) which allow us to explore a wide range of structural mismatch and subsequent strain state of the films. Furthermore, the use of two compounds with different conduction bandwidth [W_0 (LSMO5) > W_0 (LCMO5)] allows us to study the impact of this parameter on the evolution of the magnetic and transport phase diagram vs strain. In both LSMO5 and LCMO5 films strain is found to produce sizable structural modification and radically different effects on the magnetic and electric

*greta.radaelli@mail.polimi.it

†fontcuberta@icmab.es

properties that we correlate with bandwidth-depending strain-induced orbital/magnetic ordering.

This knowledge should be valuable in view of the engineering of heterostructures involving half-doped manganites for application in oxide electronics devices. In fact, due to their position close to the ferromagnetic-metallic/antiferromagnetic-insulating transition in the phase diagram of $La_{1-x}A_xMnO_3$ manganites, they are intrinsically highly sensitive to external perturbations, such as electric and magnetic fields or strain. This makes them very appealing for the realization of devices, such as tunneling junctions, where the externally induced phase transition can result in a giant variation of macroscopic magnetic or transport properties.

II. EXPERIMENT

Thin films of $La_{0.5}Sr_{0.5}MnO_3$ (LSMO5) and $La_{0.5}Ca_{0.5}MnO_3$ (LCMO5), of different thickness, were epitaxially grown by pulsed laser deposition (PLD) on (001)-oriented single-crystalline substrates (a pseudocubic notation is used for those which are not cubic): (a) $DyScO_3$ (abbreviated hereafter as DSO, lattice constant of 3.940 Å); (b) $SrTiO_3$ (STO, 3.905 Å); (c) (La,Sr)(Al,Ta)O_3 (LSAT, 3.870 Å); (d) $LaAlO_3$ (LAO, 3.792 Å); (e) $YAlO_3$ (YAO, 3.720 Å). For LSMO5 (3.858 Å [11]) the mismatch values referred to bulk compounds, $\delta = (a_{\text{substrate}} - a_{\text{manganite}})/a_{\text{manganite}} \times 100\%$, are +2.13% (DSO), +1.22% (STO), +0.31% (LSAT), −1.71% (LAO), and −3.58% (YAO). For LCMO5 films (3.830 Å) the mismatch values δ are +2.87% (DSO), +1.96% (STO), +1.04% (LSAT), −0.99% (LAO), and −2.87% (YAO). Mismatch values for LSMO5 and LCMO5 on different substrates are summarized in Table I. The films have been deposited at 725 °C in 0.2 mbar oxygen pressure with subsequent free cooling in 100 mbar oxygen pressure. The growth rate has been calibrated by measuring, by x-ray reflectivity (XRR), the thickness of some *ad-hoc* prepared films. Subsquently, the number of laser pulses has been fixed and kept constant for all growth sequences. Laser fluence has been verified to be constant for all growth processes. Data for films of 20 nm thickness are fully described in the main body of the paper; data for 36-nm-thick films are instead included in the Supplemental Material N°2 [12].

TABLE I. The calculated mismatch values (δ) and the in-plane (a) and out-of-plane (c) lattice parameters measured by q plots and θ-2θ scans, respectively, for LSMO5 and LCMO5 films grown on five different substrates. Data for LSMO5 on LSAT, which cannot be evaluated from the θ-2θ scan, have been estimated by assuming a full in-plane strain and assuming unit cell conservation.

	LSMO5			LCMO5		
Substrate	δ (%)	$a_{q\text{-plot}}$ (Å)	$c_{\theta\text{-}2\theta}$ (Å)	δ (%)	$a_{q\text{-plot}}$ (Å)	$c_{\theta\text{-}2\theta}$ (Å)
DSO	+2.13	3.925	3.761	+2.87	3.91	3.733
STO	+1.22	3.907	3.803	+1.96	3.907	3.74
LSAT	+0.31	3.87	3.833	+1.04	3.865	3.77
LAO	− 1.71	3.802	3.965	− 0.99	3.793	3.88
YAO	− 3.58	3.864	3.891	− 2.87	3.833	3.90

The x-ray diffraction (XRD) and XRR measurements were carried out using Cu-$K\alpha$ radiation, in a Siemens D-5000 diffractometer and a Rigaku RU-200B diffractometer. Reciprocal space maps (RSMs) were collected using a Bruker 1T8 Advance diffractometer equipped with a bidimensional detector. Atomic force microscopy (AFM) images, taken using an Agilent 5100 system in tapping mode, were used to characterize the surface morphology. Magnetization data were recorded with a superconducting quantum interference device (SQUID), in field-cooling (FC) conditions with an applied field parallel to the film surface. Electrical resistivity and magnetoresistance were measured either in the four- or two-probes configuration, using a physical property measurement system (PPMS) from QD.

III. RESULTS AND DISCUSSION

A. Structural characterization

Figures 1(a) and 1(b) show the θ-2θ XRD pattern around the (002) reflections of LSMO5 and LCMO5 films grown on all used substrates, respectively. The substrates (002) reflections are identified by vertical lines and by the corresponding name of the substrate. Solid vertical lines (purple) indicate the position of the (002) reflections of LSMO5 and LCMO5 films and the dashed vertical lines indicate the position of the bulk (002) LSMO5 or LCMO5 peaks. Broader angular range scans do not show any reflection different than (00l) thus indicating that films are fully c-axis textured. In most cases (except films on YAO) the Laue fringes are well visible indicating excellent film planarity and constant thickness. Horizontal arrows in Figs. 1(a) and 1(b) emphasize the shift between the measured position of the peaks of LSMO5 and LCMO5 films and the corresponding bulk positions and reflects the strain state of the films. As shown in Fig. 1(a), LSMO5 on YAO and LAO films have the (002) reflections at lower 2θ angles than bulk LSMO5; this indicates an out-of-plane expansion as expected from the lattice mismatch ($\delta < 0$) imposing a compressive in-plane stress. On the contrary, in LSMO5 on STO and DSO, the (002) reflections occur at higher 2θ angles than bulk LSMO5; this indicates a shrinking of the out-of-plane cell parameter, in agreement with the lattice mismatch ($\delta > 0$) imposing a tensile in-plane stress. In the case of LSMO5 on LSAT, the (002) reflection of the film overlaps with the (002) reflection of the substrate as expected from their small mismatch. Note that the position of the (002) peak from LSMO5 film on YAO is very close to the bulk one, while from the mismatch value ($\delta = -3.58\%$) it should occur at a lower angle than that of the film of LSMO5 on LAO ($\delta = -1.71\%$). This observation indicates that LSMO5 on YAO is almost relaxed.

Overall, data for LCMO5 films on the different substrates [Fig. 1(b)] show the same trends. However, a remarkable difference exists: As the unit cell of bulk LCMO5 is smaller than that of LSMO5, the stress-compressed films are less compressed and the tensile-stressed films are more tensile strained. The calculated out-of-plane lattice constants from these XRD data ($c_{\theta\text{-}2\theta}$) are included in Table I. The data for LSMO5 on LSAT, which cannot be evaluated from the θ-2θ scan, has been estimated by assuming a full in-plane strain and assuming unit cell conservation.

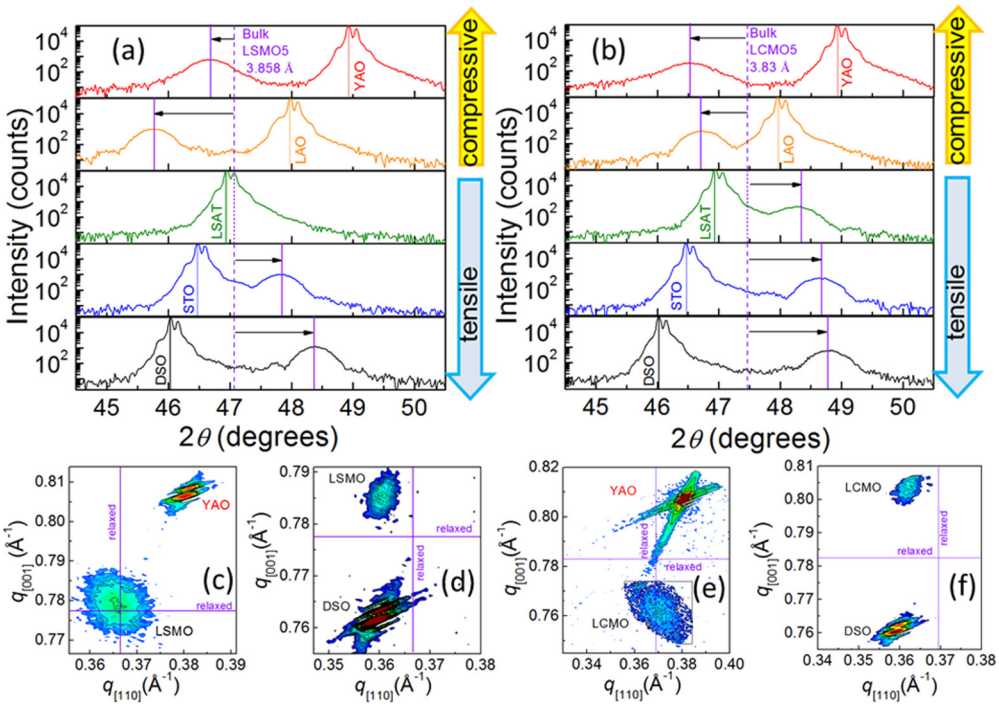

FIG. 1. (Color online) Top panels: θ-2θ XRD scans of the (002) reflections for LSMO5 (a) and LCMO5 (b) films grown on five different substrates. Bottom panels: reciprocal space maps around (113) reflections for LSMO5 films on YAO (c) and DSO (d) substrates and for LCMO5 films on YAO (e) and DSO (f) substrates.

To determine the in-plane cell parameters, reciprocal space maps around the (113) reflections were collected. In Figs. 1(c)–1(f) we show the maps for the two extreme cases for each manganite: LSMO5 and LCMO5 films on DSO substrate, with in-plane tensile stress, and on YAO substrate, with in-plane compressive stress. In the first case [DSO substrate, Figs. 1(d) and 1(f)] it can be appreciated that the reflections from the films have $q_{[110]}$ values that roughly coincide with those of the substrate and are definitely far from the relaxed position (vertical line), while the $q_{[001]}$ values of the spots from the films and the substrate are quite different. This means that the in-plane lattice constant (a) of the film expands and closely matches that of the substrate, whereas the out-of-plane lattice constant (c) shrinks. In the case of LSMO5 and LCMO5 on YAO [Figs. 1(c) and 1(e), respectively] the position of the spots of the films are closer to those of the corresponding bulk compounds, indicating lattice relaxation. From the position of the (113) film's reflection we calculated the in-plane ($a_{q\text{-plot}}$) and out-of-plane ($c_{q\text{-plot}}$) lattice parameters. The $a_{q\text{-plot}}$ data are included in Table I, where we also show the c parameter arising from θ-2θ scans ($c_{\theta\text{-}2\theta}$). Since θ-2θ scans have higher resolution than q plots in determining out-of-plane cell parameters, we used $c_{\theta\text{-}2\theta}$ and $a_{q\text{-plot}}$ to calculate the tetragonality ratio c/a and the unit cell volume values [$V_{uc} = (a_{q\text{-plot}})^2 c_{\theta\text{-}2\theta}$], shown in Fig. 2. These c/a values reflect the actual strain state of the films and they will be used accordingly, in the following.

In Fig. 2(a) we show the dependence of c/a (left axis, solid symbols) and V_{uc} (right axis, empty symbols) of the epitaxial LSMO5 films on the mismatch with the substrates. The corresponding data for LCMO5 are shown in Fig. 2(b). We first note that in these 20-nm-thick films, the c/a ratio (solid symbols) can be changed from 0.958 to 1.043 for LSMO5 and from 0.954 to 1.023 for LCMO5 films, going, in both cases, from DSO to LAO substrate. Note that for LSMO5 films on YAO, the c/a value is close to the bulk one ($c/a \approx 1$, unstrained state) which is expected from the high mismatch ($\approx$3.58%), and in agreement with this, relaxation is observed in Figs. 1(c) and 1(e). Very small tetragonality ($c/a \sim 1$) also occurs when the mismatch is very small, as for LSMO5 on LSAT substrates. In the other cases, elongation ($c/a > 1$) or contraction ($c/a < 1$) is found when the mismatch is compressive or tensile, respectively. On the other hand, it can be also appreciated that neither for LSMO5 nor for LCMO5, the unit cell volume of the films (empty symbols) is preserved under strain (the corresponding bulk values are indicated by red dashed horizontal lines) but varies with the mismatch. V_{uc} is close to the bulk value for the films with smaller strain ($c/a \approx 1$) but systematically enlarges upon tensile or compressive epitaxial strain. The very same trend is observed in LSMO5 [Fig. 2(a)] and LCMO5 [Fig. 2(b)]. These data do not allow to discriminate if this variation reflects a nonvolume preserving pure elastic response of the LSMO5 and LCMO5 lattices under strain, or some sort of chemical self-adaptation (i.e., nonstoichiometry, to minimize the strain-related elastic energy), as reported in related oxides [13,14]. The atomic force microscopy images of all the films (see Supplemental Material N°1 [12]) indicate a surface roughness of about (or smaller than) a single perovskite unit cell ($\approx$0.4 nm) which does not vary significantly by the strain.

Thicker LSMO5 films (36 nm) show the same structural and morphologic trends (see Supplemental Material N°2 [12]).

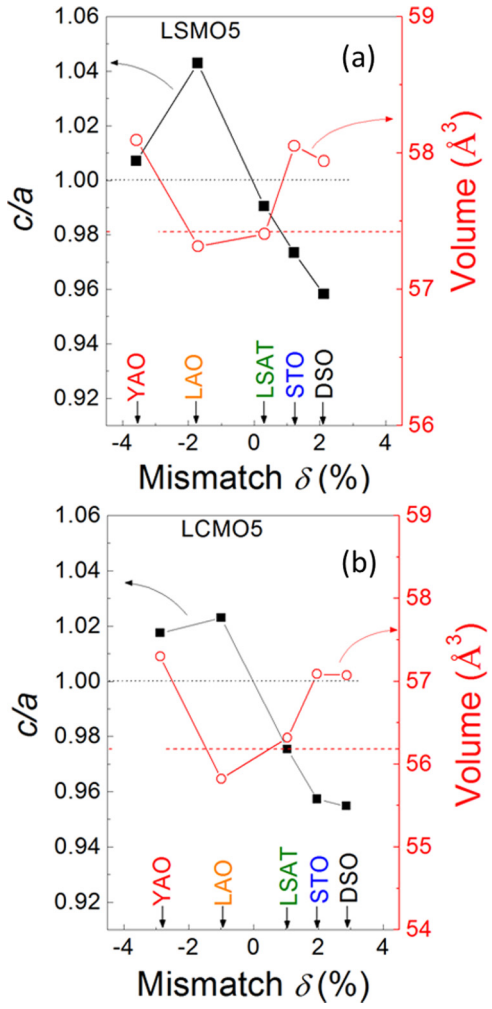

FIG. 2. (Color online) Dependence of tetragonality ratio c/a (left axis, solid squares) and unit cell volume (right axis, empty circles) values of the epitaxial LSMO5 (a) and LCMO5 (b) films on the structural mismatch imposed by various substrates (YAO, LAO, LSAT, STO, and DSO). Dotted and dashed horizontal lines indicate the corresponding bulk values of c/a and volume, respectively.

B. Magnetization, electrical transport, and magnetotransport properties

Figures 3(a)–3(c) display the temperature-dependent magnetization $M(T)$ [measured in field-cooling conditions (FC) using an in-plane field $H = 1$ kOe], the field-dependent magnetization $M(H)$ (at 50 K), and the in-plane resistivity $\rho(T)$ of the LSMO5 films on different substrates, respectively. Figures 3(d)–3(f) show the corresponding data for LCMO5. In these figures the magnetic data for films on DSO are not included because the strong magnetic contribution of the substrate largely masks the film contribution (see Supplemental Material N°3 [12]).

As shown in Fig. 3(a) the LSMO5 film grown on a matching substrate [LSAT ($c/a = 0.990$, green circles)] displays a FM transition at the Curie temperature (T_C) around 345 K, and a large magnetization (about 400 emu/cm^3) at the lowest temperature which is similar to that reported for bulk LSMO5 [15,16]. LSMO5 on YAO ($c/a = 1.007$, red triangles), with a small compressive strain, also displays a similar FM behavior but with a somewhat reduced magnetization (≈300 emu/cm^3) and T_C decreased to about 335 K. The low-temperature enhancement of magnetization is due to paramagnetic impurities in the YAO substrate. When increasing further the compressive strain, as in LSMO5/LAO ($c/a = 1.043$, orange stars), the $M(T)$ data show a severely depressed magnetization (<50 emu/cm^3) and a peak at about 190 K, which indicates a transition from paramagnetic to antiferromagnetic AF state at the Néel temperature. The tensile-strained LSMO5/STO ($c/a = 0.973$, blue squares) film displays a much suppressed magnetization although there is a ferromagnetic contribution rising below $T_C \approx 285$ K. The magnetization data of films on DSO (see Supplemental Material N°3 [12]) are consistent with an antiferromagnetic behavior. The $M(H)$ loops [Fig. 3(b)] (measurements have been performed at 50 K to minimize the paramagnetic contribution from the substrates) display the same trends as observed in the $M(T)$ data [Fig. 3(a)], namely a sharp suppression of ferromagnetism by strain.

As shown in Fig. 3(c), the in-plane resistivity $\rho(T)$ is also reflecting the change of the magnetic ground state of LSMO5 under strain. It is clear that films grown on roughly matched substrates [LSMO5/LSAT ($c/a = 0.990$, green circles)] or quasirelaxed [LSMO5/YAO ($c/a = 1.007$, red triangles)] are metallic: resistivity decreases when decreasing temperature. This is also true for the film grown on the moderately tensile-stressing substrates LSMO5/STO ($c/a = 0.973$, blue squares). In contrast, a compressive strain [LSMO5/LAO ($c/a = 1.043$, orange stars)] drives the LSMO5 into an insulating phase, evidenced by the negative $\rho(T)$ slope at 300 K. By increasing further the tensile strain [LSMO5/DSO ($c/a = 0.958$, black rhombi)], $\rho(T)$ displays a rather weak temperature dependence, with a metallic-like slightly positive $d\rho(T)/dT$ slope down to about 200 K, and a rapid increase at lower temperature. It can also be appreciated in Fig. 3(c) that the room-temperature resistivity of the LSMO5/DSO film is larger than that of the LSMO5/LAO film. This, at first sight, puzzling behavior is due to the presence of fracture microcracks in the highly tensile-stressed LSMO5/DSO film (see Supplemental Material N°4 [12]). The dependencies of the remanent magnetization (at 50 K) and resistivity (at 230 K) of LSMO5 films on the tetragonality ratio c/a are collected in Figs. 4(a) and 4(b) (black solid squares).

Summarizing, LSMO5 films have a FM ground state that shifts towards AF ordering when increasing the tetragonal distortion, either $c/a > 1$ or $c/a < 1$. However, it is clear in Figs. 3(a) and 3(b) that the transition from FM to AF does not produce a full suppression of magnetization but some ferromagnetic contribution persists in the films. This is fully consistent with a PS scenario where FM/AF phase coexistence is modulated by strain [6]. On the other hand, LSMO5 films, either unstrained or under tensile strain, show metallic behavior; a compressive strain, instead, produces an insulating ground state.

The LCMO5 films display a very different response. As shown by the $M(T)$ and $M(H)$ data in Figs. 3(d) and 3(e), respectively, all films have a very small magnetization signaling PS with predominant regions in the AF ground state, most noticeable in LCMO5/LAO film ($c/a = 1.023$, orange stars) where a peak in the magnetization [Fig. 3(d)] at about 170 K

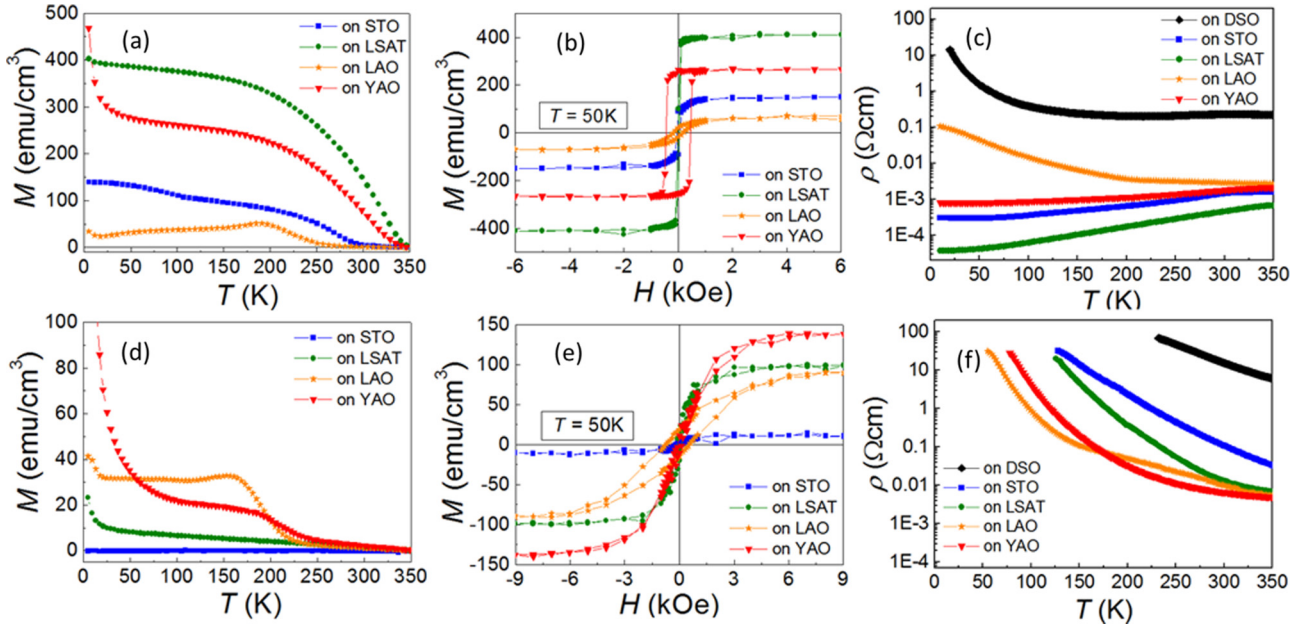

FIG. 3. (Color online) Temperature-dependent magnetization $M(T)$ (FC conditions; in-plane field H=1 kOe), field-dependent magnetization $M(H)$ loops (at 50 K, H in plane) and temperature-dependent resistivity $\rho(T)$ of the LSMO5 (a)–(c) and LCMO5 (d)–(f) films on different substrates (DSO, STO, LSAT, YAO, and LAO), respectively.

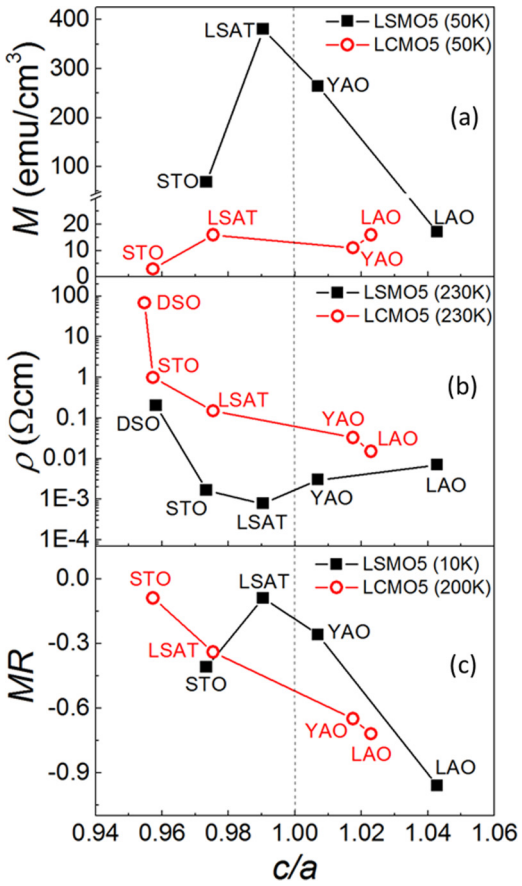

FIG. 4. (Color online) Dependencies of the (a) remanent magnetization (at 50 K), extracted from $M(H)$ loops, (b) resistivity (at 230 K), extracted from $\rho(T)$ curves, and (c) magnetoresistance at 90 kOe (at 10 and 200 K) for LSMO5 (solid squares) and LCMO5 (empty circles) films, respectively, on the tetragonality ratio c/a.

suggests a paramagnetic to AF phase transition; the $M(T)$ plateau at lower temperatures signals the presence of a small FM contribution (about 30 emu/cm^3) while the increase of $M(T)$ for very low temperature is due to the paramagnetic contribution of the LAO substrate. A similar behavior is displayed by LCMO5/YAO ($c/a = 1.017$, red triangles) in Fig. 3(d) where we observe a very weak magnetic contribution (about 20 emu/cm^3) and the strong paramagnetic contribution of the YAO substrate. In contrast, the magnetization of LCMO5/STO ($c/a = 0.957$, blue squares) is negligible indicating a pure AF phase. Figure 3(e) shows the $M(H)$ loops measured at $T = 50$ K. These plots confirm the presence of a residual FM phase in the LCMO5 films although the strong paramagnetic substrate contribution does not permit to easily appreciate the trend of M vs strain which is more evident in $M(T)$ data in Fig. 3(d). In summary, all LCMO5 films are AF. Films compressively strained, such as LCMO5/LAO and LCMO5/YAO, display major residual FM contributions, indicative of PS, which are not appreciated in the magnetization response of the films with tensile strain.

The $\rho(T)$ data in Fig. 3(f) show that LCMO5 films, irrespectively of the substrate, are insulating. Inspection of data in Fig. 3(f) indicates that the resistivity increases when decreasing c/a: from LAO, $c/a = 1.023$ in-plane compressive strain, to DSO, $c/a = 0.955$ in-plane tensile strain.

The overall trends in magnetization (at 50 K) and resistivity (at 230 K) vs tetragonality of LCMO5 films are better seen in Figs. 4(a) and 4(b) (red empty symbols). When comparing the magnetic and transport results obtained for LSMO5 films and for LCMO5 films we can observe that (a) for LSMO5 films a compressive strain drives its FM/M ground state towards a PS state with predominance of AF/I regions, whereas tensile strains promote the formation of AF/M regions, and (b) for LCMO5 films, the ground state is AF/I and strain does not

change it. The existence of FM PS regions in LCMO5 films is more evident in films under compressive strain. Probably this is also the reason why the resistivity of these films is lower than that of their tensile-strained counterparts.

The coexistence of AF/I and FM/M phases in these films can be monitored by the magnetic-field-dependent resistivity reported in Fig. 5. During the measurement the magnetic field was increased from 0 Oe to 90 kOe and then decreased back to zero. Whereas for LSMO5 low-temperature (10 K) measurements were possible owing to the relative low resistivity of this series of samples, the insulating character of the LCMO5 films precluded measurements below 200 K. To compare results for films on different substrates, resistivity values were normalized to the values measured at $H = 0$ Oe at the beginning of the measurement (ρ_0). In Fig. 5(a) are shown the results obtained at 10 K for LSMO5 films on different substrates. All the samples present negative magnetoresistance ($MR = [\rho(H)–\rho_0]/\rho_0$). It turns out that the *MR* clearly correlates with the c/a ratio, being minimal for $c/a \approx 1$ and increasing when c/a departs from $\approx$1. For LSMO5/LSAT ($c/a = 0.990$, green circles), LSMO5/YAO ($c/a = 1.007$, red triangles), LSMO5/STO ($c/a = 0.973$, blue squares), and LSMO5/LAO ($c/a = 1.04$, orange stars) the corresponding *MR* values at 90 kOe are −10%, −20%, −40%, and −90%, respectively. In other words, *MR* is minimal for films that are ferromagnetic and display a metallic-like conductivity. This is the expected behavior, at low temperature, for an epitaxial film of a double exchange manganite presenting PS. Naturally, the presence of FM/M regions in the already metallic AF films (LSMO5/STO) makes the *MR* more pronounced. Finally, the *MR* gets even larger in insulating AF films containing FM/M patches such as LSMO5/LAO. Here field-induced magnetization orientation of FM/M clusters and its eventual expansion by charge-ordering suppression under magnetic field lead to a large *MR* [17]. The hysteretic $\rho(H)$ observed in LSMO5/LAO fully agrees with this picture. No hysteresis was observed in the other LSMO5 films.

The *MR* data of the LCMO5 films, shown in Fig. 5(b), follow a fully consistent trend. The *MR* is very small for films which are purely AF, without traces of FM regions (i.e., LCMO5/STO). The *MR* increases slightly in LCMO5/LSAT, where the FM contribution also increases. The larger increase of MR for LCMO5/YAO and LCMO5/LAO films is also in agreement with the presence of a larger fraction of FM/M regions. This also explains why the resistivity of these films is smaller than that of those films with a smaller fraction of FM/M regions (LCMO5/STO, LSAT). In these measurements, there is no significant hysteresis probably due to relatively high temperature (200 K) used in the measurements. For completeness, we show in Fig. 4(c) the dependence of the *MR* (90 kOe) on c/a for all films.

Finally, we show in Fig. 6 the temperature dependence of the resistivity of all samples measured at different magnetic fields ($H = 0$ and 90 kOe). These data clearly show the presence of a significant negative magnetoresistance in most of the films. In fact, a detailed inspection of data shows that for films with a minor phase separation, LSMO5 films on LSAT is the clearest example [Fig. 6(a)], a negative *MR* is seen close to the Curie temperature, vanishing at lower temperature. This is the common colossal magnetoresistance (CMR) in manganites, attributed to a complex percolative regime associated to nanoscale phase-separated phases occurring close to the Curie temperature. In contrast, in the more strained films (such LSMO5 on LAO) an additional rapid increase of the negative

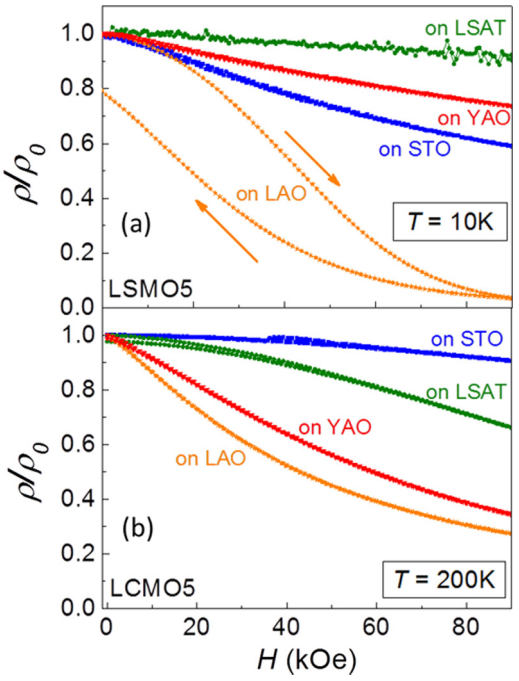

FIG. 5. (Color online) Magnetic-field-dependent resistivity of (a) LSMO5 (at 10 K) and (b) LCMO5 (at 200 K) films grown on different substrates. Data were recorded by increasing H from 0 Oe to 90 kOe and then decreasing back to zero. Except for LSMO5/LAO, hysteresis is negligible. Resistivity values were normalized to the value measured at 0 Oe at the beginning of the measurement (ρ_0).

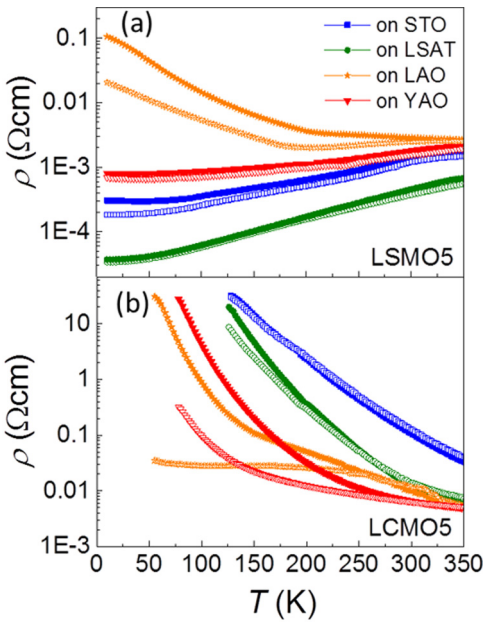

FIG. 6. (Color online) Temperature dependence of the resistivity of (a) LSMO5 and (b) LCMO5 films on different substrates (STO, LSAT, YAO, and LAO) measured at $H = 0$ Oe (full symbols) and $H = 90$ kOe (empty symbols).

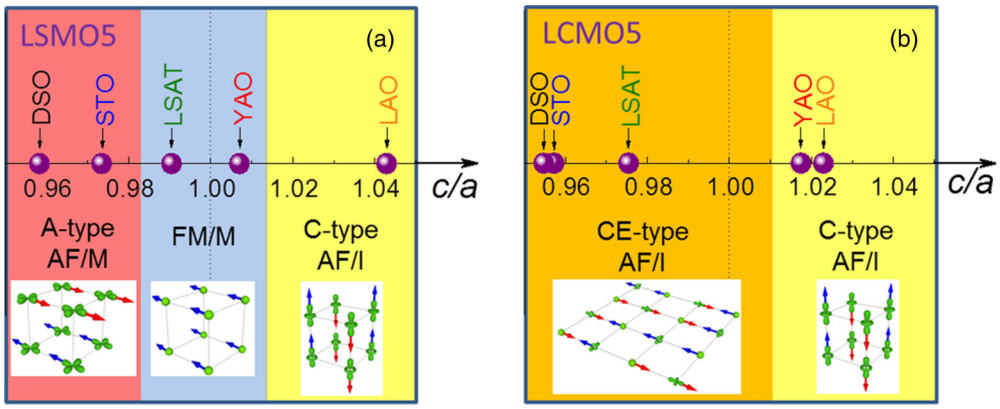

FIG. 7. (Color online) Experimentally obtained slice of the phase diagram of the $La_{1-x}Sr_xMnO_3$ (a) and $La_{1-x}Ca_xMnO_3$ (b) in the plane of c/a and doping level x corresponding to $x = 0.5$. Yellow zones indicate C-type AF/I ground state, red zone indicates A-type AF/M ground state, blue zone indicates FM/M ground state, orange zone indicates CE-type AF/I ground state. Insets are adapted from Fig. 1 of Ref. [5].

MR is observed below about 200 K. This is the signature of the existence of the AF-FM phase separation occurring at this temperature. The stronger *MR* signals the field-induced transition of some AF regions into FM under the magnetic field. The observation of these two different CMR effects are in full agreement with theoretical predictions [18] and some early experiments on manganite single crystals [19]. Similar trends can be identified in the LCMO5 films shown in Fig. 6(b).

Summarizing, the *MR* data are consistent with a distinctive PS in LSMO5 and LCMO5. In LSMO5, when increasing the strain, the M/FM state, characteristic of the unstrained condition, is gradually replaced by an AF/I (compressive) or AF/M (tensile) phase although patches of the M/FM phase remain. For LCMO5, although all films are AF and insulating, the magnetization and *MR* data also confirm the coexistence of ferromagnetic and metallic regions.

IV. DISCUSSION

The results presented above provide a comprehensive view of strain effects on wideband (LSMO5) and narrow-band (LCMO5) half-doped manganites. Let us now discuss the magnetotransport phase control of LSMO5 and LCMO5 epitaxial films enabled by epitaxial strain.

We focus first on LSMO5. As shown by data in Fig. 4(a), the weakly strained LSMO5 films are FM and the tetragonal distortion imposed by strain reduces the film magnetization and pushes the systems towards an AF ground state irrespectively of the sign of the strain. Transport data show that whereas compressive strain (as in LSMO5/LAO) induces insulating character, this is not the case for films under moderate tensile strain (LSMO5/STO) which are clearly metallic down to the lowest temperatures. On the basis of the similar inter-relation between the lattice strain and the magnetic and charge-transport properties obtained by Y. Konishi *et al.* [3] and based on the phase diagram of $La_{1-x}Sr_xMnO_3$ as a function of c/a [4,5], we assign the ground states of the respective films to FM/M (LSAT, YAO), A-type AF/M (STO), and C-type AF/I (LAO). It should be noted that the A-type AF state is metallic only in the lateral (in-plane) direction, whereas the C-type AF state is nonmetallic. It is illustrated in the phase diagram of Fig. 7(a) that for films on LAO, YAO, LSAT, and STO, fully agrees with early predictions by Fang *et al.* [4] and Baena *et al.* [5]. In contrast, when LSMO5 is grown on DSO and has the largest strain-induced basal-plane expansion, the film is found to be metallic at high temperature, although with a remarkably small $d\rho(T)/dT$ slope, and shows a fast rise of $\rho(T)$ at lower temperature. Therefore, although this film could be labeled as an A-type AF/M, the $\rho(T)$ behavior is intriguing. Due to the stronger tensile strain of LSMO5/DSO film, it could be argued that the in-plane d-d hopping integral is reduced by increasing the Mn-O-Mn bond length and, accordingly, this should lead to a reduction of the corresponding bandwidth and the FM double exchange term in the magnetic interaction, thus leaving behind only the antiferromagnetic superexchange term, and correspondingly an insulating antiferromagnetic state could be realized. However, LSMO5/STO and LSMO5/DSO films differ only modestly on tetragonality ($c/a = 0.973$ and 0.955, respectively) and therefore the difference in their low-temperature transport behavior (metallic vs insulating) does not seem directly related to the intrinsic band-narrowing effect produced by strain. Therefore, either minute band narrowing drives the Fermi level below the mobility edge of the quasi-two-dimensional conducting band of x^2-y^2 parentage or the conductivity is suppressed by extrinsic effects, such as dislocations or point defects that may be certainly more abundant in the most strained films. Measurements performed on four different LSMO/DSO films gave similar results. As mentioned above, in LSMO5/DSO films regular fracture lines have been clearly observed and it is likely that an even larger density of smaller cracks exists within the films thus giving rise to an extrinsic insulating-like behavior at low temperature. The narrowed bandwidth simply would amplify the impact of these microstructural defects on the measured $\rho(T)$.

All LCMO5 films are found to be essentially AF and insulators, irrespectively of their strain state [Figs. 4(a) and 4(b)]. We recall here that bulk LCMO5 commonly displays a FM phase with a $T_C \approx 250$ K and an antiferromagnetic charge-ordered state at $T_{CO} \approx 180$ K [6,7]; however, it has been shown that the LCMO5 ground state can be better described as a magnetically phase-separated system with ferromagnetic/metallic and antiferromagnetic/insulating phases coexisting in a wide temperature range, in amounts largely

depending on measuring conditions and sample preparation [20–22]. Theoretical calculations suggest that in bulk LCMO5 the insulating charge-ordered state (*CE*-type) is the ground state which appears to be remarkably robust. In fact, *CE* is the ground state for unstrained and tensile-strained LCMO5, whereas the *C*-type AF can stabilize under large compressive strain [5]. In all cases and in agreement with the present experimental data, the insulating character of LCMO5 is preserved. Accordingly, we assign the ground states of the films having $c/a > 1$ (i.e., LCMO5/LAO and LCMO5/YAO) to the *C*-type AF/I state, as depicted in Fig. 7(b). Regarding the tensile-strained regions ($c/a < 1$), our results are compatible with the predicted *CE*-type ordering as observed at low temperature in bulk LCMO5 [6,7].

V. CONCLUSIONS

We have reported a comprehensive study of epitaxial strain on thin films of half-doped manganites $La_{0.5}Sr_{0.5}MnO_3$ (LSMO5) and $La_{0.5}Ca_{0.5}MnO_3$ (LCMO5) on a variety of substrates. It is found that epitaxial strain imposed by the substrates promotes pseudotetragonal cells with c/a ratio that can be largely tuned: $0.958 < c/a < 1.04$ (LSMO5) and $0.954 < c/a < 1.023$ (LCMO5). The ground state of bulk LSMO5 is recovered in thin films grown on well matched substrates, and the corresponding thin films are ferromagnetic and metallic. In contrast, compressive biaxial strain leads to the emergence of an antiferromagnetic insulating state that we identify as *C*-type AF and tensile strain leads to an uncommon antiferromagnetic and metallic (in-plane) phase, reflecting an *A*-type AF spin ordering. The reduced metallicity of LSMO5 upon stronger tensile strain is attributed to the combined effect of conduction band narrowing and the ubiquitous presence of extended planar defects in the film. In the narrower-bandwidth LCMO5 oxide, the epitaxial strain imposed by the substrates drives in all cases the films into an AF and insulating state, with minor effects on conductivity or magnetization. Coexistence of phase-separated AF and FM regions has been identified in strained LSMO5 films and, to a lesser extent, in LCMO5. It thus follows that strain has remarkably different effects on LSMO5 and LCMO5 that mainly arise from the difference in the electronic bandwidth and the corresponding ground state. Therefore we anticipate that half-doped manganites, if integrated on piezoelectric stressors or tunnel junctions in conjunction with ferroelectric layers, will respond differently depending on their bandwidth. For instance, we envisage any field effects should dominate in LCMO5-based barriers whereas piezo-induced strain may have a more prominent role on LSMO5. Although more investigations are needed to definitely settle the microscopic nature of spin and orbital ordering in these films, the findings here reported should help to design more responsive devices, such as multifunctional tunnel barriers with improved response.

ACKNOWLEDGMENTS

We acknowledge financial support by the Spanish Government (Projects No. MAT2011-29269-CO3 and No. NANOSELECT CSD2007-00041), Generalitat de Catalunya (Project No. 2009 SGR 00376), and the Italian Ministry of Research (Project No. FIRB RBAP115AYN). We also are thankful to Luis Brey for helpful comments.

[1] J. D. Burton and E. Y. Tsymbal, Phys. Rev. Lett. **106**, 157203 (2011).
[2] Y. W. Yin, J. D. Burton, Y.-M. Kim, A. Y. Borisevich, S. J. Pennycook, S. M. Yang, T. W. Noh, A. Gruverman, X. G. Li, E. Y. Tsymbal, and Qi Li, Nat. Mater. **12**, 397 (2013).
[3] Y. Konishi, Z. Fang, M. Izumi, T. Manako, M. Kasai, H. Kuwahara, M. Kawasaki, K. Terakura, and Y. Tokura, J. Phys. Soc. Jpn. **68**, 3790 (1999).
[4] Z. Fang, I. V. Solovyev, and K. Terakura, Phys. Rev. Lett. **84**, 3169 (2000).
[5] A. Baena, L. Brey, and M. J. Calderón, Phys. Rev. B **83**, 064424 (2011).
[6] A. J. Millis, Nature (London) **392**, 147 (1998).
[7] P. Schiffer, A. P. Ramirez, W. Bao, and S.-W. Cheong, Phys. Rev. Lett. **75**, 3336 (1995).
[8] Y. M. Xiong, G. Y. Wang, X. G. Luo, C. H. Wang, X. H. Chen, X. Chen, and C. L. Chen, J. Appl. Phys. **97**, 083909 (2005).
[9] M. Malfait, I. Gordon, V. V. Moshchalkov, Y. Bruynseraede, G. Borghs, and P. Wagner, Phys. Rev. B **68**, 132410 (2003).
[10] A. Antonakos, D. Lampakis, E. Liarokapis, M. Filippi, W. Prellier, G. H. Aydogdu, and H.-U. Habermeier, J. Phys.: Condens. Matter **20**, 434232 (2008).
[11] Measured by XRD on our target and in good agreement with literature: J. Spooren, R. I. Walton, and F. Millange, J. Mater. Chem. **15**, 1542 (2005).
[12] See Supplemental Material at http://link.aps.org/supplemental/10.1103/PhysRevB.89.075107 for N°1: Atomic Force Microscopy characterization of $La_{0.5}Sr_{0.5}MnO_3$ and $La_{0.5}Ca_{0.5}MnO_3$ films; N°2: $La_{0.5}Sr_{0.5}MnO_3$ films 36 nm thick grown on different substrates; N°3: Magnetic characterization of $La_{0.5}Sr_{0.5}MnO_3$ grown on $DyScO_3$; N°4: Scanning electron microscopy (SEM) images for $La_{0.5}Sr_{0.5}MnO_3$ grown on $DyScO_3$.
[13] S. Estradè, J. M. Rebled, J. Arbiol, F. Peiró, I. C. Infante, G. Herranz, F. Sánchez, J. Fontcuberta, R. Córdoba, B. G. Mendis, and A. L. Bleloch, Appl. Phys. Lett. **95**, 072507 (2009).
[14] J. Gazquez, S. Bose, M. Sharma, M. A. Torija, S. J. Pennycook, C. Leighton, and M. Varela, Appl. Phys. Lett. Mater. **1**, 012105 (2013).
[15] Z. Jirák, J. Hejtmánek, K. Knížek, M. Maryško, V. Šíma, and R. Sonntag, J. Magn. Magn. Mater. **217**, 113 (2000).
[16] Y. Tokura and Y. Tomioka, J. Magn. Magn. Mater. **200**, 1 (1999).
[17] H. Kuwahara, Y. Tomioka, A. Asamitsu, Y. Moritomo, and Y. Tokura, Science **270**, 961 (1995).
[18] H. Aliaga, D. Magnoux, A. Moreo, D. Poilblanc, S. Yunoki, and E. Dagotto, Phys. Rev. B **68**, 104405 (2003).
[19] Y. Tokura, H. Kuwahara, Y. Moritomo, Y. Tomioka, and A. Asamitsu, Phys. Rev. Lett. **76**, 3184 (1996).
[20] J. C. Loudon, N. D. Mathur, and P. A. Midgley, Nature **420**, 797 (2002).
[21] P. Levy, F. Parisi, G. Polla, D. Vega, G. Leyva, H. Lanza, R. S. Freitas, and L. Ghivelder, Phys. Rev. B **62**, 6437 (2000).
[22] G. Allodi, R. De Renzi, F. Licci, and M. W. Pieper, Phys. Rev. Lett. **81**, 4736 (1998).